

Modeling the effect of feed gas perturbation on CO₂ removal using potassium glycinate in a membrane contactor

Nayef Ghasem (✉ nayef@uaeu.ac.ae)

United Arab Emirates University

Article

Keywords: CFD simulation, membrane contactor, CO₂ removal, oscillating flow, overall mass transfer coefficient, potassium glycinate

Posted Date: May 31st, 2022

DOI: <https://doi.org/10.21203/rs.3.rs-1665568/v1>

License:  This work is licensed under a Creative Commons Attribution 4.0 International License.

[Read Full License](#)

Modeling the effect of feed gas perturbation on CO₂ removal using potassium glycinate in a membrane contactor

Nayef Ghasem

Department of Chemical & Petroleum Engineering, United Arab Emirates University,

P.O.BOX 15551, Al-Ain City, UAE

Email: nayef@uaeu.ac.ae

Abstract

Gaseous-solvent membrane absorption process is a smart approach for removing impurities such as CO₂ present in natural gas, flue gas, and biogas into aqueous solvents. Potassium glycinate solvent has better CO₂ absorption performance compared to traditional solvents. However, hollow fiber membrane design has limitations, as the presence of the membrane adds additional resistance to mass transfer compared to conventional solvent absorption. To reduce the effect of this additional resistance, it is necessary to increase the mass transfer in the gas and solvent phase boundary layers. This study aims to increase the mass transfer in the gas phase layer without interfering with membrane structure by oscillating the velocity of the feed gas. Consequently, an unsteady state mathematical model was developed and solved using Comsol Multiphysics. The simulation results reveal an optimal oscillation frequency that enables high CO₂ removal to be achieved. Under specific operating conditions and without feeding disturbance, the maximum removal rate was about 30%. Applying a feed gas oscillation frequency of 0.05 Hz doubles this to about 70% for CO₂ removal.

Keywords: CFD simulation; membrane contactor; CO₂ removal; oscillating flow; overall mass transfer coefficient; potassium glycinate.

1. Introduction

Power plants established on fossil fuels are the main source of CO₂ emission and hence a primary environmental concern and change in climate¹. Reducing CO₂ emissions from power plants through carbon capture is a reasonable solution. Various CO₂ capture techniques have been implemented, including cryogenic separation, solvent absorption, and, lately, membrane solvent-gas contactor²⁻⁴. Membrane solvent-gas technology got the advantages of gas separation and compact size with resealable CO₂ absorption^{5,6}. By contrast, membrane separation technologies introduce mass transfer resistances in the liquid phase, gas phase, and membrane layer⁷. Membrane contactors were also used for purposes other than absorption. The membrane was used to strip dissolved gases other than CO₂, such as methane from wastewater treatment anaerobic effluents, natural gas, and flue gas⁸⁻¹¹. The treatment method was used in converting chemical oxygen to biogas. As methane is the primary source of biogas, the membrane separation process is utilized to liberate dissolved methane from anaerobic effluents¹². Potassium glycinate solvent is an effective solvent as an aqueous solution used to absorb CO₂ inside a solvent-gas hollow fiber membrane contactor^{13,14}. Experimentally, the feed gas oscillating flow was induced and improved the mass transfer correlations in terms of Sherwood number. The study revealed that inducing mixing with the gas phase enhanced the absorption rate in the membrane contactor¹⁵. They were recycling the anesthetic agents used in daily clinical routines that required the removal of CO₂ to enable the reuse of xenon. A membrane contactor with amino-acid ionic liquid as a solvent was utilized to remove CO₂ from the noble gas Xenon anesthesia circuits¹⁶. The membrane distillation module has a necessary practical implementation. Accordingly, computational fluid dynamics and design of experiments were performed on a membrane distillation.

Simulation results revealed the length of the membrane module length has strong impact on the flux¹⁷. Mathematical modeling was performed in a membrane contactor for CO₂

absorption in different solvents. Various solvents were used in the CO₂ absorption process. Various solvents were used, such as 4-diethylamino-*n*-butanol (DEAB), diethanolamine (DEA), and methyldiethanolamine (MDEA) were used in hollow fiber modules. DEAB absorption rate was competitive with MEA aqueous solutions¹⁸. The gas velocity in a membrane gas absorption plays a significant role in improving the separation performance. The addition of baffles improves the SO₂ absorption performance at the critical velocity¹⁹. Membrane manufacturing materials have a significant influence on membrane separation performance.

A hollow fibrous membrane of a PVDF/CaCO₃ composite was synthesized for CO₂ removal²⁰. The results indicate that incorporating CaCO₃ nanoparticles into PVDF enhanced the porosity, surface roughness, and gas permeation rate, thus increasing the CO₂ adsorption flux²¹. Regeneration of ammonia utilized in CO₂ capture is low relative to the MEA. Ammonia is a desirable solvent for CO₂ removal from the flue and natural gas²². The ammonia-based CO₂ capturing process in a hollow fiber membrane contactor shows a better mass transfer performance in the dense membrane phase than conventional gas/liquid absorption processes²³. Membrane outer diameter has a substantial impact on membrane separation performance. Membrane modules with fibers more fabulous than 1.2 mm in diameter increased mass transfer resistance and decreased the membrane contactor specific area per unit volume. A membrane with a 0.9 mm outer diameter or less is more suitable²⁴. A significant parametric study for different physical solvents revealed the importance of physical solvents in absorption and regeneration processes compared to the packed column conventional technology²⁵. The objective of developing gas-liquid membrane conductors is to reduce the capital cost and energy consumption of conventional CO₂ absorbers and separation columns^{26–28}. Membrane material, the type of solvent, the configuration of solvent and gas placed in the lumen or shell side, and the operating temperature played a significant role in conquering the technical

challenges of membrane wetting and resulted in a decrease in the mass transfer coefficient ^{29,30}. Nanoparticles such as SiO₂ and Al₂O₃ along with MEA aqueous solution were useful in reducing the energy consumption in the CO₂ stripping ³⁰. The highest mass transfer resistance was in the liquid phase. The increased in liquid velocity increased the desorption flux ³¹.

Based on the above, there are difficulties in increasing the mass transfer coefficient based on the membrane structure, composition, and configuration. Accordingly, the current work focused on modeling and simulating the gaseous solvent membrane contactor based on the oscillating feed gas flow rate to increase the percentage of CO₂ removal without affecting the membrane structure and composition.

2. Mathematical model

A two-dimensional unsteady state mathematical model has been developed to describe the adsorption of carbon dioxide from methane in potassium glycinate (PG) solvent using a hollow fiber membrane adsorption process under the influence of an oscillating gas flow. The potassium glycinate solvent is fed to the lumen side at $z = 0$, and the gas stream enters the shell counter currently at $z = L$ (Figure 1). Certain assumptions were considered, such as isothermal operation, laminar flow, and Henry's law is applicable at the liquid-gas interface and non-wetting mode (gas-filled the membrane pores).

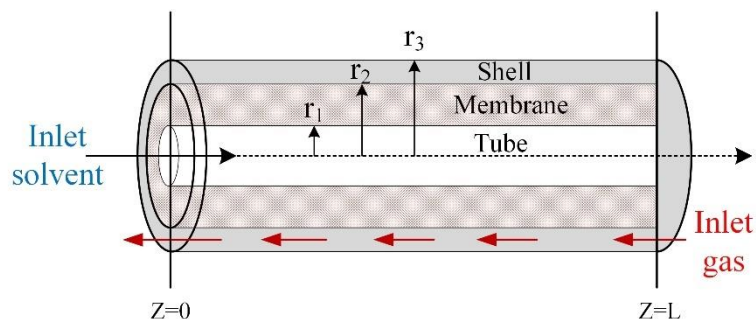


Figure 1. Schematic diagram and the membrane contactor model domain

2.1 Hollow fiber lumen (solvent flow)

The unsteady steady-state gas transport in the lumen solvent side ($i: CO_2, CH_4$):

$$\frac{\partial C_{i,t}}{\partial t} = -D_{i,t} \left[\frac{\partial}{\partial r} \left(\frac{1}{r} \frac{\partial C_{i,t}}{\partial r} \right) + \frac{\partial^2 C_{i,t}}{\partial z^2} \right] + r_{i,t} + v_{z,t} \frac{\partial C_{i,t}}{\partial z} \quad (1)$$

The aqueous solution velocity ($v_{z,t}$):

$$v_{z,t} = \frac{2Q_t}{n\pi r_1^2} \left(1 - \left(\frac{r}{r_1} \right)^2 \right) \quad (2)$$

The boundary conditions:

at $z = 0$, $C_{CO_2,t} = 0$ (fresh solvent)

at $z = L$, $\frac{\partial C_{CO_2,t}}{\partial z} = 0$ (convective flux)

at $r = 0$, $\frac{\partial C_{CO_2,t}}{\partial r} = 0$ (symmetry)

at $r = r_1$, $C_{CO_2,t} = m C_{CO_2,m}$ (solubility of CO_2 in PG)

The forward reaction rate is expressed as follows ³².

$$r_{CO_2} = -2.42 \times 10^{16} \exp\left(\frac{-8544}{T}\right) \exp(0.44 C_{Pg}) C_{Pg} C_{CO_2} \quad (3)$$

Where $T(K)$ is the liquid temperature, C_{Pg} is the concentrations of PG, and C_{CO_2} is the concentration of CO_2

2.2 Membrane skin

The unsteady steady-state gas diffusion across the membrane walls:

$$\frac{\partial C_{i,m}}{\partial t} = -D_{i,m} \left[\frac{\partial}{\partial r} \left(\frac{1}{r} \frac{\partial C_{i,m}}{\partial r} \right) + \frac{\partial^2 C_{i,m}}{\partial z^2} \right] \quad (4)$$

The boundary conditions of the membrane skin:

at $z = 0$, $\frac{\partial C_{i,m}}{\partial z} = 0$ (insulation)

at $z = L$, $\frac{\partial C_{i,m}}{\partial z} = 0$ (insulation)

at $r = r_1$, $D_{i,m} \frac{\partial C_{i,m}}{\partial r} = D_{i,t} \frac{\partial C_{i,t}}{\partial r}$

at $r = r_2$, $C_{i,m} = C_{i,s}$

2.3 The shell of the module (gas stream)

The unsteady steady-state gas concentration in the shell side:

$$\frac{\partial C_{i,s}}{\partial t} = -D_{i,s} \left[\frac{\partial}{\partial r} \left(\frac{1}{r} \frac{\partial C_{i,s}}{\partial r} \right) + \frac{\partial^2 C_{i,s}}{\partial z^2} \right] + v_{z,s} \left(\frac{\partial C_{i,s}}{\partial z} \right) \quad (5)$$

The perturbation of the velocity of the gas on the shell side ³³:

$$v_{z,s} = v_{zm} \sin(\omega t) \left\{ 1 - \left(\frac{r_2}{r_3} \right)^2 \right\} \left\{ \frac{\left(\frac{r}{r_3} \right)^2 - \left(\frac{r_2}{r_3} \right)^2 - 2 \ln \left(\frac{r}{r_2} \right)}{3 + \left(\frac{r_2}{r_3} \right)^4 - 4 \left(\frac{r_2}{r_3} \right)^2 + 4 \ln \left(\frac{r_2}{r_3} \right)} \right\} \quad (6)$$

Where ω is the frequency. The appropriate boundary conditions:

$$z = z_1, C_{i,s} = C_{i,0} \quad (\text{initial concentration})$$

$$z = z_0, \frac{\partial^2 C_{i,sa}}{\partial z^2} = 0 \quad (\text{convective flux})$$

$$r = r_2, D_{i,s} \frac{\partial C_{i,sa}}{\partial r} = D_{i,ms} \frac{\partial C_{i,ma}}{\partial r} \quad (\text{diffusive flux})$$

$$r = r_3, \frac{\partial C_{i,sa}}{\partial r} = 0$$

The radius of the free surface (r_3), is expressed as follows:

$$r_3 = r_2 \left(\frac{1}{1-\varphi} \right)^{0.5} \quad (7)$$

The module void fraction (φ):

$$\varphi = \frac{R^2 - n r_2^2}{R^2} \quad (9)$$

R , r_2 , n are the inner radius of the module, fiber outer radius, and the number of fibers, respectively. Q_t is the solvent circulation volumetric rate and n is the number of fibers. Table 1 lists the characteristics of the hollow fiber membrane module.

Table 1. Membrane characteristics used in the mathematical model

Number of fibers	20
------------------	----

Hollow fiber inner radius, mm	0.21
Hollow fiber, outer radius, mm	0.55
Module insider radius, m	0.008
Module length, m	0.25

3. Mass transfer coefficient, K_G

The total mass transfer coefficient, K_G ($\frac{kmol}{m^2.s.kPa}$) is estimated based on the two-phase theory as the ratio of the CO_2 absorption flux (J_{CO_2}) to the solute concentration gradient between gas and liquid³⁴. The CO_2 absorption flux (J_{CO_2}) is calculated based on the following expression³⁵.

$$J_{CO_2} (mol/m^2.s) = \frac{Q_g(y_{CO_2,in} - y_{CO_2,out})}{A} \quad (10)$$

Where Q_g is the gas molar flow rate (mol/s) (assuming inlet and exit flow rate are the same; neglecting the effect of the amount of CO_2 being absorbed on the gas flow rate), $y_{CO_2,in}$, and $y_{CO_2,out}$ are the inlet and exit mole fraction of CO_2 , and A is a gas-liquid interface contact area based on the internal diameter of the hollow fiber. The total mass transfer coefficient is calculated as follows³⁶:

$$K_G (m/s) = \frac{J_{CO_2}}{C_{g,Lm}} \quad (11)$$

Where K_G symbolizes the overall mass transfer coefficient in the gas phase, $C_{g,Lm}$ is the average log mean concentration of CO_2 in the bulk gas phase of outlet and inlet concentration³⁷.

$$C_{g,lm} = \frac{C_{CO_2,in} - C_{CO_2,out}}{\ln(C_{CO_2,in}/C_{CO_2,out})} \quad (12)$$

The exit gas concentration ($C_{CO_2,out}$) is determined using the boundary line integration built in Comsol 5.6.

4. Results and Discussion

4.1 Model validation

The model predictions were validated using the membrane characterization and the experimental data available from literature ³⁴. The model validation was performed by comparing the overall mass transfer coefficient between the experimental data and the simulation predictions. As per the experimental data used in the model validation, the gas stream was fed to the lumen side and the solvent to the shell side, opposite to the configuration shown in Figure 1. The model prediction of the experimental data is acceptable. The model predictions revealed that further increase in gas velocity had insignificant effects on the total gas mass transfer coefficients due to the decrease in the gas residence time, despite the formation of a thin mass transfer layer formed with the increase in the gas feed rate.

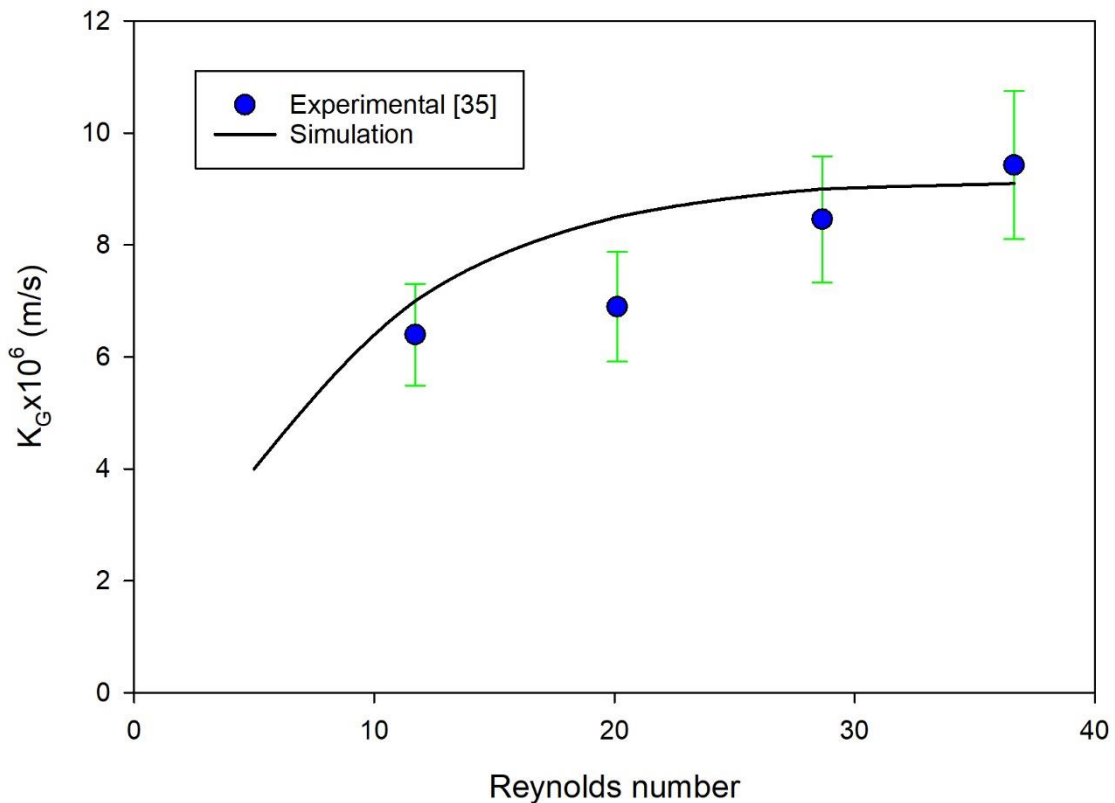


Figure 2. Model validation with the experimental data from ³⁴.

Figure 2 shows a comparison of model prediction for case if the gas feed stream was introduced to the lumen or shell side. A comparison of the gas feed rate between tube side and shell side discovered that introducing the gas in the module shell side enhanced the overall mass transfer coefficient compared to gas being introduced into the tube side (Figure 3). Accordingly, the rest of the results are based on gas flow fed into the shell side and liquid solvent into the tube side. This configuration match up most of the experimental work performed where liquids are introduced to the lumen side of the membrane module ³⁷. The increase in the mass transfer coefficient of the case where gas is fed into the shell side is attributed to the increase in the better mixing, and the increase in residence time when gas. Accordingly, the simulation is performed based on the data available in Table 1 and the gas is introduced into the shell side.

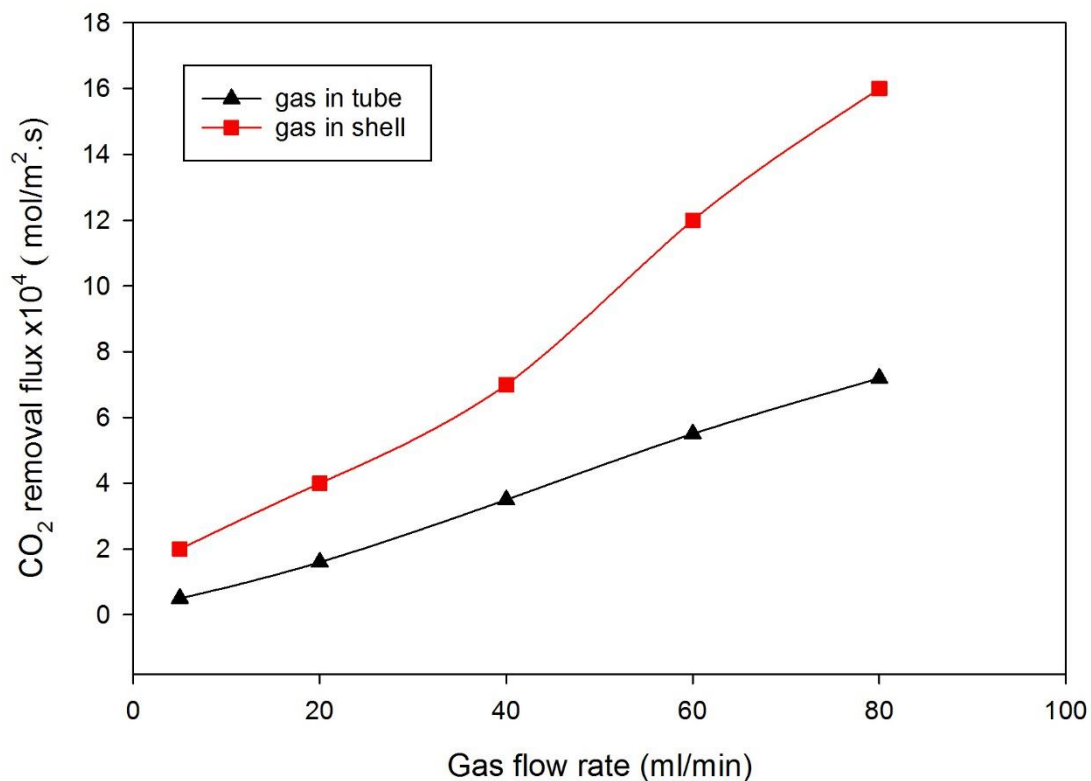


Figure 3. Comparison between the oscillatory gas flows in the shell and tube sides at fixing other operating condition.

4.2 Gas feed perturbation.

Figure 4 shows the gas feed velocity coefficient at different sinusoidal frequencies. Since the absorption occurs in a gas-liquid membrane system that is stabilized very rapidly, a time range of 60 seconds is investigated. The frequency range is maintained while increasing the speed gradually and reaching the maximum point in 60 seconds. For example, at a frequency of 0.03, the gas speed gradually increased until it reached its maximum value. Frequencies (other than 0.05) cause the velocity to reach the maximum speed more than once in an oscillatory manner within the studied range.

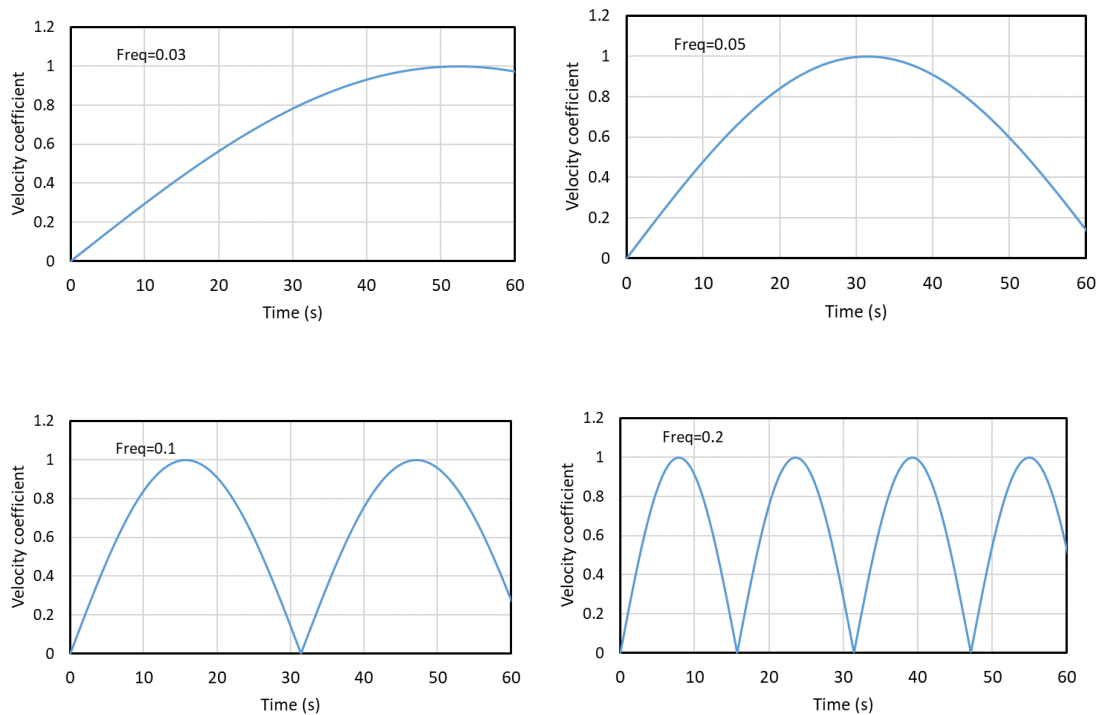


Figure 4. Gas feed velocity coefficient at various sinewave frequencies.

Under sinusoidal operating conditions, the velocity of the feed gas at different frequencies is described in Figure 5. The figure exposed the effect of the feed gas sinusoidal frequency on CO₂ concentration along the shell side of the membrane unit. The lowest concentration profile

is at a frequency of 0.05 HZ. The smaller the CO₂ concentration indicates, the higher the percent removal of CO₂ from the natural gas mixture.

Figure 6 depicts the effect of sinewave frequencies on the percent removal of CO₂ from the feed gas stream. The figure showed that CO₂ removal percentage is very low at a frequency of 0.03 percent, and the removal rate reached the maximum at a frequency of 0.05. Further increase in the frequencies causes a decline in the percentage of CO₂ removal. That is attributed to the sinusoidal number of cycles. At a frequency of 0.2, the velocity coefficient increases within the investigated interval of 60 seconds around four times. The results indicated that an oscillation frequency of 0.05, achieves the highest CO₂ removal rate.

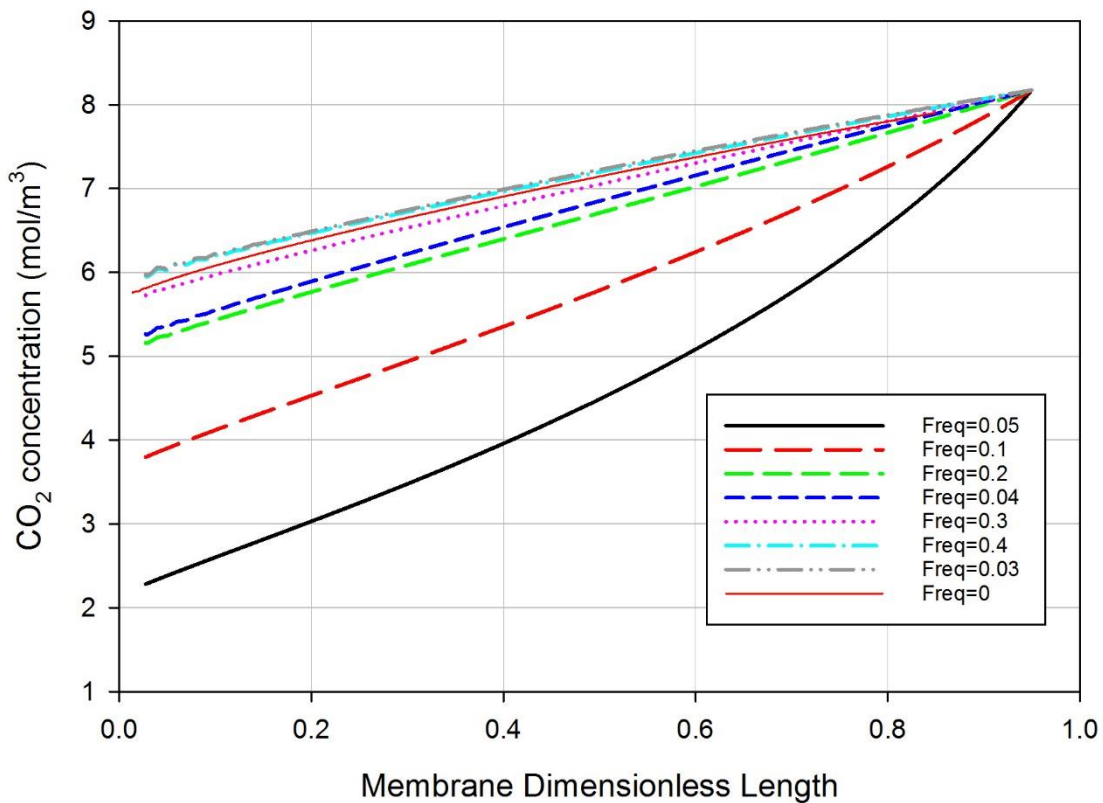


Figure 5. Effect of gas feed oscillation frequency on the CO₂ concentration profile versus membrane dimensionless length of the gas flow on the shell side. Gas feed rate 500ml/min, liquid feed rate 10 ml/min.

The cycle generated from a frequency of 0.05 shows the best removal rate as the velocity reaches the maximum and then decreases to give more room for fresher gas and increase the driving force. Further increase in the frequencies leads to the increased number of cycles with the investigated period, decreasing the residence time and not giving more time for separation. The reasonable frequency of 0.05 doubled the percentage removal because the pressure wave generated by the oscillation of the feed gas produces localized increases in the partial pressure driving force for mass transfer across the membrane. The results were in good agreement with the experimental observations available elsewhere ³⁴.

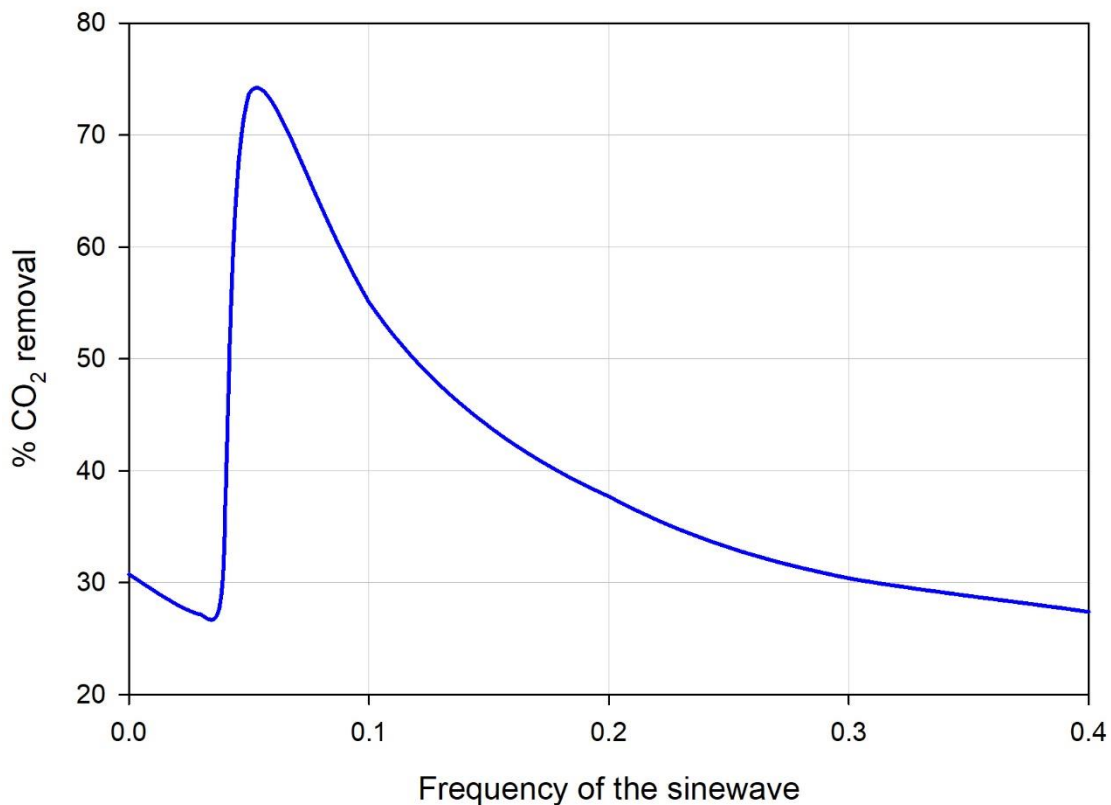


Figure 6. Effect of the sinewave frequency in the feed stream on the percent removal of carbon dioxide from the natural gas stream. The liquid feed rate is 10 ml/min; the gas feed rate is 500 ml/min.

Figure 7 shows the model predictions for the effect of a feed gas flow rate at a constant sinusoidal frequency of 0.05 on CO₂ concentrations and removal flux along the dimensionless membrane length. The figure showed that along the membrane dimensionless length, the higher the gas flow rate, the lower the CO₂ removal rate, and the higher the CO₂ removal flux. That is attributed to the fact that, an increase in the gas flow rate usually reduces the thickness of the gas boundary layer, which is supposed to enhance the mass transfer rate and increase the CO₂ removal ratio. In contrast, at the same time, an increase in the feed gas flow rate reduces the residence time, which reduces the rate of mass transfer and thus reduces the rate of CO₂ absorption along with the membrane gas-phase compartment (membrane unit envelope side). Similar results were reported by other researchers ³⁸⁻⁴⁰. This indicates that the residence time strongly impacts the CO₂ percent removal rate. The increase in the CO₂ removal flux with gas flow rate is attributed to the increased amount of CO₂ being absorbed with gas flow rate. Accordingly, residence time strongly affects CO₂ removal compared to gas mass transfer intensification ⁴¹.

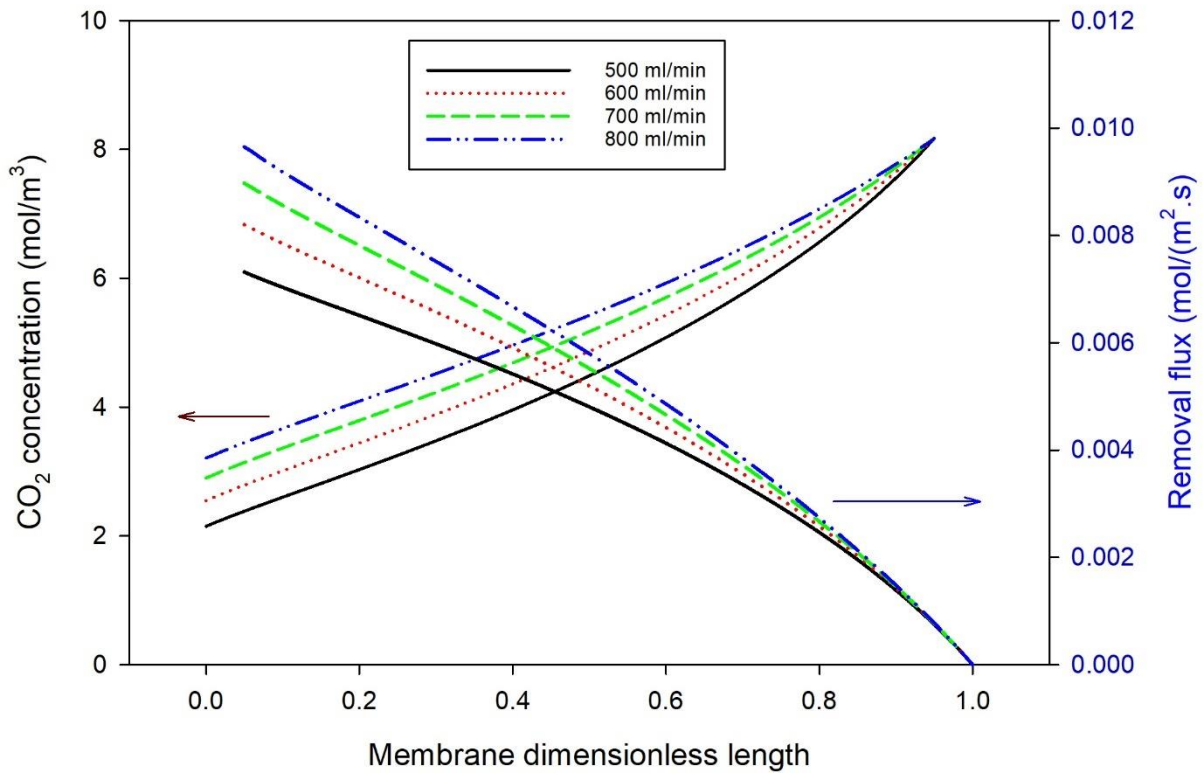


Figure 7. Effect of feed gas flow rate on the CO₂ concentrations and removal flux at the optimum frequency of 0.05.

Figure 8 indicates the influence of the gas feed rate at 0.05 sinusoidal frequency on the total mass transfer coefficients. The total mass transfer coefficient increased with the gas feed rate due to the increase in the amount of carbon dioxide absorbed, and the thickness of the gas boundary layer decreased with the increase in gas velocity. The total mass transfer coefficients increase with the increase in gas velocity mentioned earlier. The results are within the range of those obtained experimentally. In contrast, the effect of gas supply rate on the total mass transfer coefficient in the absence of gas supply disturbance in the sine waveform is negligible. Similar trends were observed by Yeon et al. ⁴²

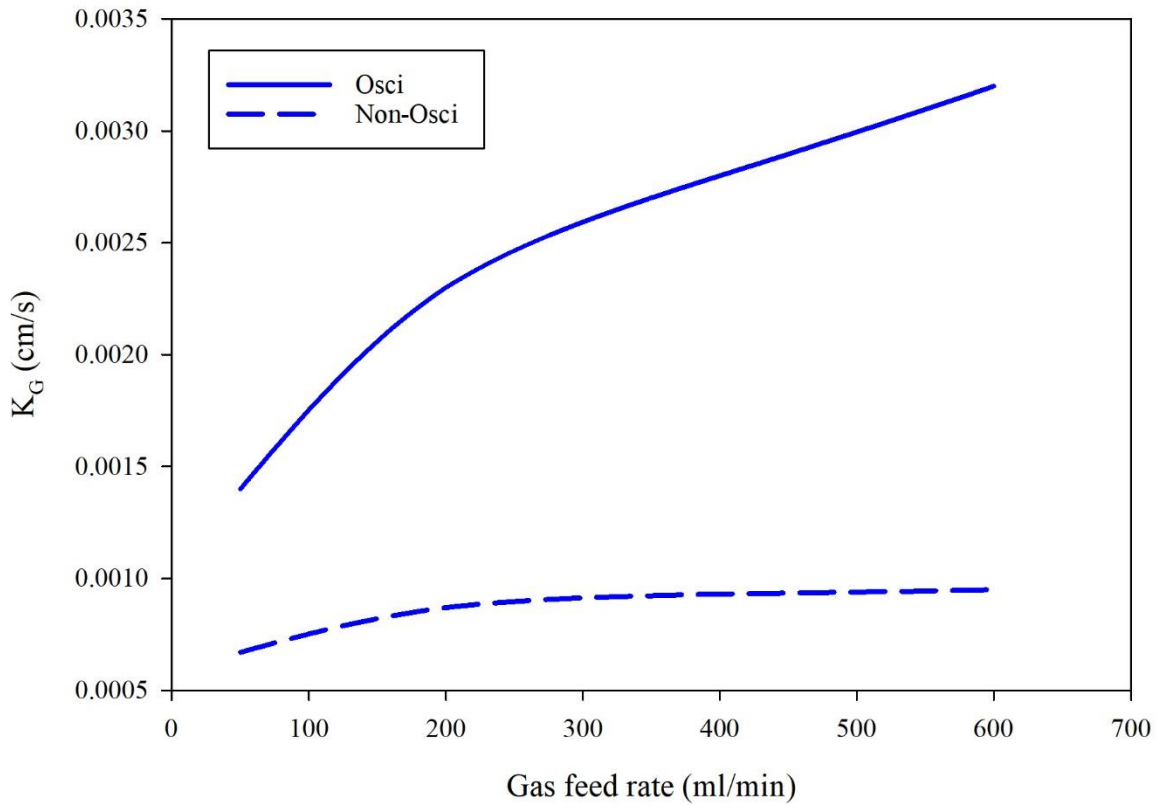


Figure 8. Effect gas feed rate on the CO₂ overall mass transfer coefficients under the optimum oscillating frequency (0.05) and in the normal conditions at a constant liquid feed rate of 10 ml/min. Gas introduced to the shell side and solvent into tube side.

Figure 9 compares the CO₂ removal flux between the oscillatory and no oscillatory gas feed rates. The figure showed that the removal percentage increased slightly in the non-oscillating operating mode at a gas feed rate up to a flow rate of 0.25 L/min. Beyond this, the change in the removal ratio with the gas feed rate is insignificant.

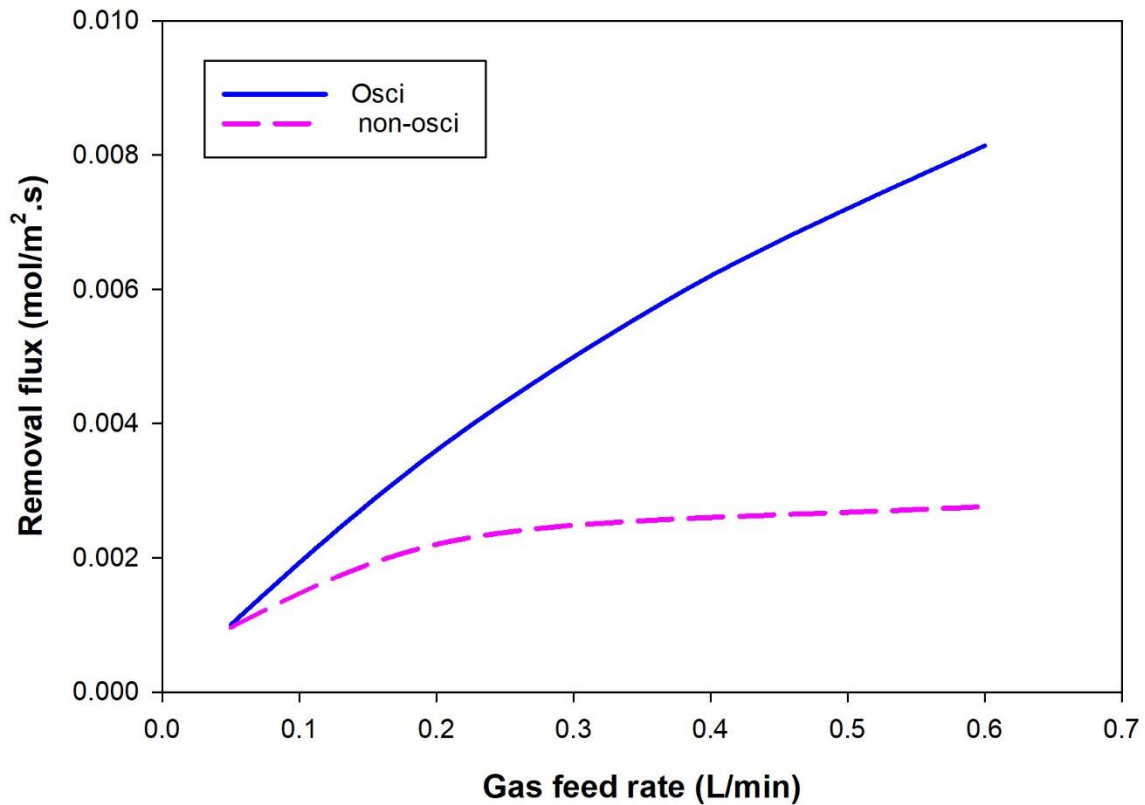


Figure 9. Influence of feed perturbation on the CO₂ removal flux under the effect of oscillatory and no oscillatory gas feed rate. The oscillating mode is at the optimum frequency of 0.05 HZ.

5. Conclusion

A two-dimensional mathematical model under non-wet mode conditions and feed gas at different sinusoidal waves with different frequencies was used to absorb CO₂ into a PG aqueous solution within a hollow fiber membrane unit. The model considers the perturbation of the inlet gas flow rate and the radial and axial diffusion within the hollow fibers, across membrane walls, and within the unit shell side. The influence of the feed gas oscillation frequency and flow rate strongly influences the CO₂ removal enhancement. The 0.05 sinusoidal frequency was the optimum value that doubled the percentage removal of CO₂.

Data Availability

All data generated or analyzed during this study are included in this published article. Additional explanations or data are available from the corresponding author on reasonable request.

References

1. Nieminen, H. *et al.* Insights into a membrane contactor based demonstration unit for CO₂ capture. *Sep. Purif. Technol.* **231**, (2020).
2. Kosaraju, P., Kovvali, A. S., Korikov, A. & Sirkar, K. K. Hollow Fiber Membrane Contactor Based CO₂ Absorption–Stripping Using Novel Solvents and Membranes. *Ind. Eng. Chem. Res.* **44**, 1250–1258 (2005).
3. Ho, C.-D., Chang, H., Lin, G.-H. & Chew, T. L. Enhancing absorption performance of CO₂ by amine solution through the spiral wired channel in concentric circular membrane contactors. *Membranes (Basel)*. **12**, (2022).
4. Zhang, H., Xue, K., Cheng, C., Gao, D. & Chen, H. Study on the performance of CO₂ capture from flue gas with ceramic membrane contactor. *Sep. Purif. Technol.* **265**, 118521 (2021).
5. Favre, E. & Svendsen, H. F. Membrane contactors for intensified post-combustion carbon dioxide capture by gas–liquid absorption processes. *J. Memb. Sci.* **407–408**, 1–7 (2012).
6. Soroodan Miandoab, E., Kentish, S. E. & Scholes, C. A. Non-ideal modelling of polymeric hollow-fibre membrane systems: Pre-combustion CO₂ capture case study. *J. Memb. Sci.* **595**, 117470 (2020).

7. Chen, G. *et al.* Mass transfer performance and correlation for CO₂ absorption into aqueous 3-diethylaminopropylamine solution in a hollow fiber membrane contactor. *Chem. Eng. Process. - Process Intensif.* **152**, 107932 (2020).
8. Ghasem, N. Modeling and Simulation of the Simultaneous Absorption/Stripping of CO₂ with Potassium Glycinate Solution in Membrane Contactor. *Membranes (Basel)*. **10**, (2020).
9. Rahim, N. A., Ghasem, N. & Al-Marzouqi, M. Absorption of CO₂ from natural gas using different amino acid salt solutions and regeneration using hollow fiber membrane contactors. *J. Nat. Gas Sci. Eng.* **26**, 108–117 (2015).
10. Ghasem, N. Chemical absorption of CO₂ enhanced by nanoparticles using a membrane contactor: Modeling and simulation. *Membranes (Basel)*. **9**, (2019).
11. Ghasem, N. Modeling and Simulation of CO₂ Absorption Enhancement in Hollow-Fiber Membrane Contactors using CNT–Water-Based Nanofluids. *J. Membr. Sci. Res.* **5**, 295–302 (2019).
12. Velasco, P., Jegatheesan, V. & Othman, M. Modeling of hollow fiber membrane contactors (HFMCs) for the recovery of dissolved methane from anaerobic effluents. *Sep. Purif. Technol.* **286**, 120488 (2022).
13. Zhang, W., Wang, Q., Fang, M., Luo, Z. & Cen, K. Experimental study on the separation of CO₂ from flue gas using hollow fiber membrane contactors with aqueous solution of potassium glycinate. *2009 Int. Conf. Energy Environ. Technol. ICEET 2009* **3**, 65–69 (2009).
14. Ghasem, N., Al-Marzouqi, M. & Rahim, N. A. Absorption of CO₂ from natural gas via gas-liquid PVDF hollow fiber membrane contactor and potassium

- glycinate as solvent. *J. Teknol. (Sciences Eng.* **69**, (2014).
15. Hosseini, E., Soroodan Miandoab, E., Stevens, G. W. & Scholes, C. A. Absorption of CO₂ from flue gas under oscillating gas flow conditions in gas-solvent hollow fibre membrane contactors. *Sep. Purif. Technol.* **249**, (2020).
 16. Martins, C. F. *et al.* Removing CO₂ from Xenon anaesthesia circuits using an amino-acid ionic liquid solution in a membrane contactor. *Sep. Purif. Technol.* **275**, 119190 (2021).
 17. Choi, J., Cho, H., Choi, Y. & Lee, S. Combination of computational fluid dynamics and design of experiments to optimize modules for direct contact membrane distillation. *Desalination* **524**, 115460 (2022).
 18. Saidi, M. Mathematical modeling of CO₂ absorption into novel reactive DEAB solution in hollow fiber membrane contactors; kinetic and mass transfer investigation. *J. Memb. Sci.* **524**, 186–196 (2017).
 19. Kong, X. *et al.* Critical gas velocity of hydrophobic ceramic membrane contactors for SO₂ absorption. *Chem. Eng. Sci.* **231**, 116327 (2021).
 20. Chen, Z., Shen, Q., Gong, H. & Du, M. Preparation of a novel dual-layer polyvinylidene fluoride hollow fiber composite membrane with hydrophobic inner layer for carbon dioxide absorption in a membrane contactor. *Sep. Purif. Technol.* **248**, (2020).
 21. Fosi-Kofal, M., Mustafa, A., Ismail, A. F., Rezaei-DashtArzhandi, M. & Matsuura, T. PVDF/CaCO₃ composite hollow fiber membrane for CO₂ absorption in gas–liquid membrane contactor. *J. Nat. Gas Sci. Eng.* **31**, 428–436 (2016).
 22. Lee, H. J. *et al.* Integrated membrane contactor absorber/regeneration column process

- for CO₂ capture with large scale module at various operating conditions. *Catal. Today* **358**, 316–323 (2020).
23. Makhloufi, C. *et al.* Ammonia based CO₂ capture process using hollow fiber membrane contactors. *J. Memb. Sci.* **455**, 236–246 (2014).
 24. Li, M. *et al.* Removal of CO₂ from biogas by membrane contactor using PTFE hollow fibers with smaller diameter. *J. Memb. Sci.* **627**, 119232 (2021).
 25. Cesari, L., Castel, C. & Favre, E. Membrane contactors for intensified gas-liquid absorption processes with physical solvents: A critical parametric study. *J. Memb. Sci.* **635**, 119377 (2021).
 26. Houliker, S. *et al.* Reconciliation of gas to liquid mass transfer in parallel and transverse flow (cross-flow) hollow fiber membrane contactors (HFMC) for CO₂ absorption. *Sep. Sci. Technol.* **56**, 129–140 (2021).
 27. Scholes, C. A., Kentish, S. E. & Qader, A. Membrane gas-solvent contactor pilot plant trials for post-combustion CO₂ capture. *Sep. Purif. Technol.* **237**, (2020).
 28. Lian, S. *et al.* Recent advances in ionic liquids-based hybrid processes for CO₂ capture and utilization. *J. Environ. Sci.* **99**, 281–295 (2021).
 29. Kim, S., Scholes, C. A., Heath, D. E. & Kentish, S. E. Gas-liquid membrane contactors for carbon dioxide separation: A review. *Chem. Eng. J.* **411**, 128468 (2021).
 30. Pang, H., Chen, Z., Gong, H. & Du, M. Fabrication of a super hydrophobic polyvinylidene fluoride–hexadecyltrimethoxysilane hybrid membrane for carbon dioxide absorption in a membrane contactor. *J. Memb. Sci.* **595**, (2020).
 31. Mohammed, H. N., Ahmed, S. M. R., Al-Naseri, H. & Al-Dahhan, M. Enhancement of CO₂ desorption from MEA-based nanofluids in membrane contactor: Simulation

- study. *Chem. Eng. Process. - Process Intensif.* **168**, 108582 (2021).
32. Eslami, S., Mousavi, S. M., Danesh, S. & Banazadeh, H. Modeling and simulation of CO₂ removal from power plant flue gas by PG solution in a hollow fiber membrane contactor. *Adv. Eng. Softw.* **42**, 612–620 (2011).
 33. Happel, J. Viscous flow relative to arrays of cylinders. *AIChE J.* **5**, 174–177 (1959).
 34. Hosseini, E., Soroodan Miandoab, E., Stevens, G. W. & Scholes, C. A. Absorption of CO₂ from flue gas under oscillating gas flow conditions in gas-solvent hollow fibre membrane contactors. *Sep. Purif. Technol.* **249**, 117151 (2020).
 35. Yan, S. *et al.* Experimental study on the separation of CO₂ from flue gas using hollow fiber membrane contactors without wetting. *Fuel Process. Technol.* **88**, 501–511 (2007).
 36. Khaisri, S., deMontigny, D., Tontiwachwuthikul, P. & Jiraratananon, R. Comparing membrane resistance and absorption performance of three different membranes in a gas absorption membrane contactor. *Sep. Purif. Technol.* **65**, 290–297 (2009).
 37. Sohaib, Q., Muhammad, A., Younas, M. & Rezakazemi, M. Modeling pre-combustion CO₂ capture with tubular membrane contactor using ionic liquids at elevated temperatures. *Sep. Purif. Technol.* **241**, 116677 (2020).
 38. Dai, Z. & Deng, L. Membrane absorption using ionic liquid for pre-combustion CO₂ capture at elevated pressure and temperature. *Int. J. Greenh. Gas Control* **54**, 59–69 (2016).
 39. Cao, Y. *et al.* Intensification of CO₂ absorption using MDEA-based nanofluid in a hollow fibre membrane contactor. *Sci. Rep.* **11**, 2649 (2021).
 40. Qazi, S. *et al.* CO₂ capture in a hollow fiber membrane contactor coupled with ionic

- liquid: Influence of membrane wetting and process parameters. *Sep. Purif. Technol.* **233**, 115986 (2020).
41. Lu, Y., Yan, J. & Dahlquist, E. *Experimental investigation on CO₂ absorption using absorbent in hollow fiber membrane contactor.* (2008).
42. Yeon, S.-H., Lee, K.-S., Sea, B., Park, Y.-I. & Lee, K.-H. Application of pilot-scale membrane contactor hybrid system for removal of carbon dioxide from flue gas. *J. Memb. Sci.* **257**, 156–160 (2005).